Torque Ripple Reduction in Interior Permanent Magnet Synchronous Machines Using the Principle of Mutual Harmonics Exclusion

Seok-Hee Han* seokheehan@wisc.edu
Thomas M. Jahns* jahns@engr.wisc.edu
Wen L. Soong+ wlsoong@eleceng.adelaide.edu.au
*University of Wisconsin – Madison, WI, USA
+University of Adelaide, Adelaide, Australia

***Abstract*— The interior permanent magnet (IPM) synchronous machine is vulnerable to developing significant amounts of current-induced ripple torque depending on the details of the machine design. Building on the contributions of earlier researchers, this paper approaches the problem of torque ripple reduction in IPM machines by applying the principle of mutual harmonics exclusion. First, this paper develops a useful analytical expression for the torque ripple that highlights the stator-rotor harmonic interactions. Next, an analytical design procedure for IPM rotors with multiple flux barriers is proposed that applies the mutual harmonics exclusion principle in combination with stator windings that use odd numbers of slots per pole pair. Finally, the technique is applied to two example IPM machines to investigate the effectiveness of this approach using finite element analysis. Promising results predict that a low peak-to-peak torque ripple can be achieved using relatively small numbers of stator slots and rotor flux barriers for the full range of current control angles, including deep flux weakening.**

Keywords - interior permanent magnet machine; torque ripple; stator-rotor harmonic interactions; mutual harmonics exclusion

I. INTRODUCTION

Interior permanent magnet (IPM) synchronous machines are vulnerable to producing significant amounts of current-induced ripple torque if the machine is not carefully designed to prevent it. The torque ripple amplitude can vary significantly depending on the operating conditions. Accordingly, this paper defines the torque ripple at each operating point as the ratio [in per cent] of the peak-to-peak torque variation to the average torque at the operating point of interest.

The peak-to-peak torque ripple for conventional IPM machines at the rated torque operating point is often approximately 20% at the current angle for maximum torque/ampere operation. For current angles corresponding to deep flux weakening, the ratio is often above 100% [3, 5–7].

Reducing torque pulsations in permanent magnet machines has received significant attention in recent years. Table I below provides a concise summary of key technical literature on torque ripple reduction. Researchers working on surface PM machines have demonstrated a promising technique for reducing the ripple torque by using a stator winding configuration with an odd number of slots per pole pair [4].

TABLE I. SUMMARY OF SELECTED LITERATURE ON TORQUE RIPPLE REDUCTION IN PM MACHINES

Ref.	*Machine type*	*Stator slots per pole pair*	*Flux barriers per pole*	*Peak-to-peak torque ripple*
[4]	SPM	9	SPM	3.4%
[2]	SynRM	18	3	4.2%
[3]	IPM	18	2	10 %
[5]	IPM	12	1	10 %
[6]	IPM	12	1	23 %
[8]	IPM	12	2	4.6 %

TABLE II. SPECIFICATIONS FOR THE EXAMPLE IPM MACHINES

Rated power P_R	1.6 kW
Rated line-to-line voltage V_R	191 Vrms
Corner speed ω_R, top speed ω_{Max}	6500 rpm, 13000 rpm
Rated torque T_R	2.4 Nm
Rated phase current I_R	7.1 Arms
Number of poles	4
Stator outer radius	36 mm
Stator inner radius	17.46 mm
Airgap length	0.42 mm
Rotor inner radius	5.06 mm
Active stack length	60 mm
Magnet remanent flux density B_r	1.04 T
Magnet relative recoil permeability	1.05

For IPM machines, other researchers have reduced the peak-to-peak torque ripple (at rated torque) to values less than 5% by increasing the number of flux barriers per pole [2]. Design features such as asymmetric flux barriers [3] or sinusoidal profiling of the rotor surface [5] have been proposed to reduce the peak-to-peak ripple torque to values in the vicinity of 10%. In recent work [8], two types of rotors were combined into one hybrid rotor structure that was then step-skewed to suppress torque ripple below 5%.

The objective of this paper is to investigate opportunities for minimizing the ripple torque in IPM machines by varying only the stator slot number and the design details of symmetrical rotor cavity configurations. Alternative proposed torque reduction techniques such as stator skewing or rotor pole shaping are not considered as part of this work. Taking advantage of the torque ripple reduction techniques presented in [2] and [4] for other types of ac machines, this paper approaches the problem by applying a principle referred to here as mutual harmonics exclusion.

0197-2618/07/$25.00 © 2007 IEEE

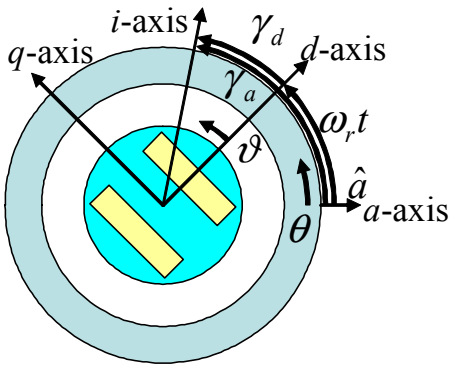

Figure 1. Definitions of key axes, current control angles, rotor position angle, and spatial coordinates in stator and rotor reference frames

First, this paper develops a useful analytical expression for the torque ripple that highlights the stator-rotor harmonic interactions. Next, an analytical design procedure for minimizing the torque ripple of IPM machines with multiple flux barriers is proposed that applies the mutual harmonics exclusion principle in combination with stator windings that use odd numbers of slots per pole pair. Finally, the technique is applied to an example IPM machine to investigate the effectiveness of this approach using finite element analysis. Several key specifications for the example IPM machines used in this paper are summarized in Table II.

II. Analytic Torque Ripple Expression and Principles of Mutual Harmonic Exclusion

This section derives the analytical expression for the instantaneous IPM torque ripple under the idealized assumptions of no magnetic saturation and closed stator slots. The stator conductors are modeled by a current sheet along the airgap surface. Compared to the existing expressions available in the literature [2] [8], the usefulness of the torque ripple expression developed in this paper is that it clearly highlights the impact of the stator-rotor harmonic interactions on the torque ripple, providing helpful insights into potential design improvements. The key axes, angles of the current excitation and the rotor position, and the spatial coordinates in the stator and rotor reference frames are illustrated in Fig. 1.

A. Winding Function

The winding function n of the stator phase winding can be expanded into its Fourier series as follows [1]:

$$n = \sum_{h=1,2,3,\cdots} n_h \cos(h\theta) \tag{1}$$

where h is the harmonic index, n_h is the h^{th}-order stator winding harmonic, and θ is the angular position [elec. rad] in the stator reference frame measured from the phase a axis. It is assumed that the winding function is even-symmetric about the phase a axis and that the winding functions of phases b and c are identical but displaced by $2\pi/3$ and $4\pi/3$ elec. rad, respectively.

B. Stator MMF

For a given set of instantaneous phase currents (i_a, i_b, i_c), the stator mmf f_s has the instantaneous spatial distribution given by

$$f_s = n(\theta) i_a + n(\theta - 120°) i_b + n(\theta - 240°) i_c \tag{2}$$

The phase current excitation can be expressed by an instantaneous current vector in the stator reference frame, expressed as

$$i_a \hat{a} + i_b \hat{b} + i_c \hat{c} \equiv i_m \angle \gamma_a \tag{3}$$

where $\hat{a}$, $\hat{b}$, $\hat{c}$ are unit vectors along the a-axis, b-axis, c-axis, i_m is the current vector amplitude, and γ_a is the current vector angle measured from the a-axis (see Fig. 1). It is assumed that the three phases windings are connected in a floating star configuration so that the three instantaneous phase currents always sum to zero:

$$i_a + i_b + i_c = 0 \tag{4}$$

Next, the Fourier series expansion of f_s can be expressed as:

$$\begin{aligned} f_s = & \sum_{h=1,4,7,\cdots} 1.5 n_h i_m \cos(h\theta - \gamma_a) + \\ & \sum_{h=2,5,8,\cdots} 1.5 n_h i_m \cos(h\theta + \gamma_a) + \\ & \sum_{h=3,6,9,\cdots} 0 \end{aligned} \tag{5}$$

Introducing $f_{s,h}$ as the notation for the h^{th}-order stator mmf harmonic and transforming the stator mmf into the rotor reference frame yields

$$f_s = \sum_{h\neq 3,6,9,\cdots} f_{s,h} \cos(h\theta \mp \omega_r t \mp \gamma_d) \tag{6}$$

where $\omega_r t$ is the instantaneous rotor angular position and γ_d is the current phase angle measured from the d-axis. The spatial derivative of f_s can be computed to be

$$\frac{df_s}{d\theta} = - \sum_{h\neq 3,6,9,\cdots} h f_{s,h} \sin(h\theta \mp \omega_r t \mp \gamma_d) \tag{7}$$

C. Rotor MMF

In response to any given set of instantaneous phase current excitation values (i_a, i_b, i_c), the presence of flux barriers inside the IPM rotor induces an instantaneous spatial distribution of rotor mmf f_r which can be expanded into a Fourier series:

$$f_r = \sum_{h\neq 2,4,\cdots} f_{r,h} \cos(h\vartheta) \tag{8}$$

where $f_{r,h}$ is the h^{th}-order rotor mmf harmonic and ϑ is the angular spatial coordinate [elec rad] in the rotor reference frame (see Fig. 1). The rotor mmf is even-symmetric about the d-axis and odd-symmetric about the q-axis. Therefore, it has no even harmonics. Transforming the rotor mmf into the stator reference frame yields

$$f_r = \sum_{h\neq 2,4,\cdots} f_{r,h} \cos(h\theta - h\omega_r t) \tag{9}$$

D. Torque ripple

Application of the Lorentz force law along the airgap surface leads to an expression for the instantaneous torque T_e:

$$T_e = r_g l_{stk} \int_{2\pi \times \frac{p}{2}} B_g df_s$$
$$= \frac{P}{2}\frac{\mu_0}{g} r_g l_{stk} \int_{2\pi} (f_r - f_s)\frac{df_s}{d\theta} d\theta \quad \text{[Nm]} \quad (10)$$
$$= \frac{P}{2}\frac{\mu_0}{g} r_g l_{stk} \left\{ \int_{2\pi} f_r \frac{df_s}{d\theta} d\theta - \int_{2\pi} f_s \frac{df_s}{d\theta} d\theta \right\}$$

where r_g is the airgap radius, l_{stk} is the active stack length, P is the number of poles, B_g is the airgap flux density and μ_0 is the permeability of the air. It follows from the machine periodicity that

$$\int_{2\pi} f_s \frac{df_s}{d\theta} d\theta = \left[\frac{1}{2} f_s^2(\theta) \right]_0^{2\pi} = 0 \quad (11)$$

On the other hand, substitution of the Fourier expansions for f_s and f_r leads to

$$\int_{2\pi} \left(-\frac{df_s}{d\theta} \right) f_r d\theta = \sum_{h=1,5,7,\cdots} \left\{ \pi h f_{s,h} f_{r,h} \sin((h \mp 1)\omega_e t \mp \gamma_d) \right\} \quad (12)$$

Separating the fundamental and harmonic components yields

$$\int_{2\pi} \left(-\frac{df_s}{d\theta} \right) f_r d\theta = \pi f_{s,1} f_{r,1} \sin(-\gamma_d) + \sum_{\substack{h=6m\mp1 \\ m=1,2,3,\ldots}} \left\{ \pi h f_{s,h} f_{r,h} \sin((h \pm 1)\omega_e t \pm \gamma_d) \right\} \quad (13)$$

Therefore, we can define the average torque T_1 by

$$T_1 = \frac{P}{2}\frac{\mu_0}{g} r_g l_{stk} \pi f_{s,1} f_{r,1} \sin(\gamma_d) \quad (14)$$

and the ripple torque T_{ripple} by

$$T_{ripple} = -\frac{P}{2}\frac{\mu_0}{g} r_g l_{stk} \pi \sum_{\substack{h=6m\mp1 \\ m=1,2,3,\ldots}} \left(h f_{s,h} f_{r,h} \sin((h \pm 1)\omega_e t \pm \gamma_d) \right) \quad (15)$$

It should be noted in this equation that the negative sign in the h index of the summation (i.e., $h=6m-1$) maps into the two positive signs in the argument of the trigonometric expression (i.e., $(h+1)\omega_e t+\gamma_d$), and vice versa.

E. Principle of Mutual Harmonic Exclusion

Using (14) and (15), the ratio of the ripple torque to the average torque is:

$$\frac{T_{ripple}}{T_1} = -\frac{1}{\sin(\gamma_d)} \sum_{\substack{h=6m\mp1 \\ m=1,2,3,\ldots}} \left(h \left(\frac{f_{s,h}}{f_{s,1}} \right) \left(\frac{f_{r,h}}{f_{r,1}} \right) \sin((h \pm 1)\omega_e t \pm \gamma_d) \right) \quad (16)$$

This compact expression clearly shows that the torque ripple is the result of the interaction between the stator and rotor mmf harmonics. Based on this formulation, the torque ripple index (*TRI*) is defined as follows:

$$TRI \equiv \sum_{\substack{h=6m\pm1 \\ m=1,2,3,\ldots}} h \frac{f_{s,h}}{f_{s,1}} \frac{f_{r,h}}{f_{r,1}} \quad (17)$$

Key observations drawn from (14) to (17) include: 1) Only stator and rotor mmf harmonics of the same order interact and contribute to the torque ripple. For example, $f_{s,5}$ interacts only with $f_{r,5}$, and not with $f_{r,7}$. 2) The harmonic orders of the torque ripple waveform are in multiples of six. Only stator and rotor mmf harmonics with orders of $6m\pm1$ contribute to the torque ripple. Therefore, for the purpose of torque ripple reduction, it is enough to consider only the stator and rotor mmf harmonics with orders of $h=6m\pm1$. 3) The products of $f_{s,h}$ and $f_{r,h}$ are amplified by the harmonic order h. Thus, higher-order mmf harmonic components can contribute disproportionately to the torque ripple amplitude. Since the stator and rotor mmf waveforms have step discontinuities caused by the stator slotting and flux barriers, special attention must be devoted to the discontinuities because of the high-frequency harmonics that they can create.

This paper presents a promising design approach for reducing the torque ripple in IPM machines by selecting the stator winding and rotor barrier configurations in carefully coordinated ways to minimize the interactions of their major mmf harmonics. The next two sections provide a detailed presentation of the analytical principles used to achieve this reduction based on the concept of mutual harmonics exclusion and this is illustrated with design examples.

III. Distributed Stator Winding Configuration with Odd Numbers of Slots-per-Pole-Pair

This section compares two classes of distributed stator winding configurations: 1) one with even numbers of slots-per-pole-pair and 2) the other with odd numbers of slots-per-pole-pair. It is shown that stator windings with odd numbers of slots-per-pole-pair are advantageous in reducing mutual interactions between the stator and rotor mmf harmonics. We will denote the number of stator slots-per-pole-pair by n_s [2]. In addition, we will name the harmonics with orders of $n_s\pm1$, $2n_s\pm1$, $3n_s\pm1$, $4n_s\pm1$ as the stator slot harmonics.

Consider first the more common case of even-numbered n_s. Figure 2a shows the winding layout for a typical distributed stator winding configuration with n_s=12 (i.e., slots-per-phase-per-pole *spp*=2). Figure 2b shows the normalized spectrum of the spatial stator mmf distribution for this winding configuration multiplied by the corresponding harmonic index h, reflecting the appearance of this factor in the torque ripple expressions found in (16) and (17). Only the harmonic components ($h=6m\pm1$) that interact with rotor mmf harmonics of the same order to produce ripple torque are plotted.

The harmonic order multiplication in the torque ripple equation has the effect of amplifying the slot harmonics ($n_s\pm1$, $2n_s\pm1$, $3n_s\pm1$) so that their amplitudes match that of the fundamental component. This observation suggests that the stator slot harmonics are particularly potent components for contributing to the ripple torque. Review of the results in the preceding section indicates that the rotor mmf has only odd-numbered harmonics due to the geometrical symmetry. Since all of the stator slot harmonics ($n_s\pm1$, $2n_s\pm1$, $3n_s\pm1$) are also odd-numbered if n_s is even-numbered, there is a major opportunity for undesirable interactions between the stator and rotor mmf harmonic components that produce ripple torque.

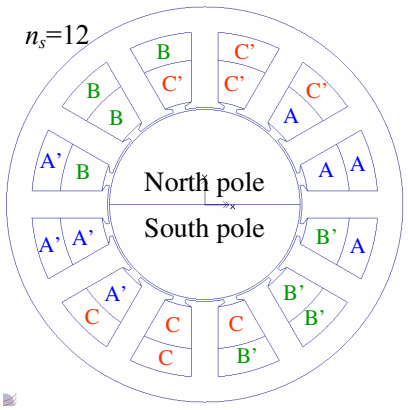

(a) Winding configuration of two poles

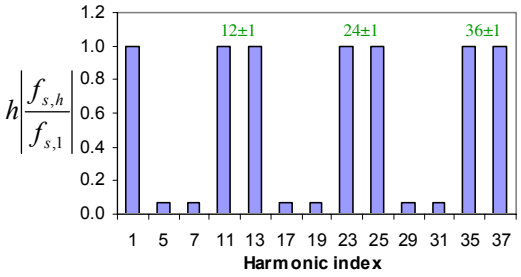

(b) Normalized stator mmf multiplied by harmonic index

Figure 2. Stator winding layout and the normalized stator mmf spectrum multiplied by the harmonic index h for n_s=12 with 2 poles.

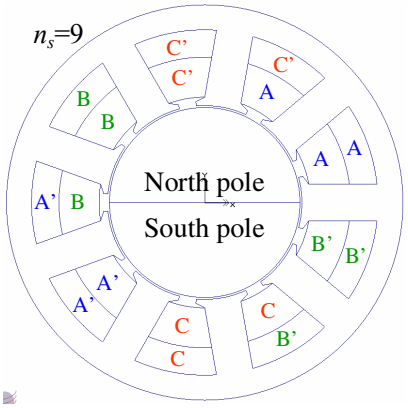

(a) Winding configuration of two poles

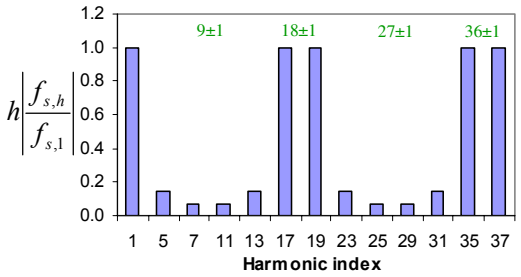

(b) Normalized stator mmf multiplied by harmonic index

Figure 3. Stator winding layout and the normalized stator mmf spectrum multiplied by the harmonic index h for n_s=9 with 2 poles.

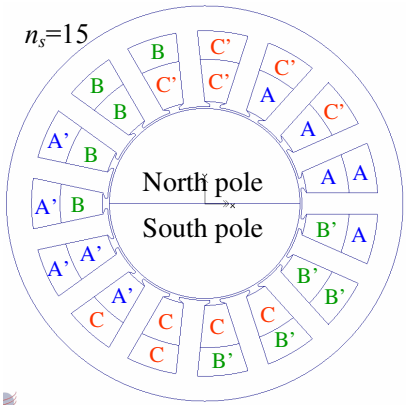

(a) Winding configuration of two poles

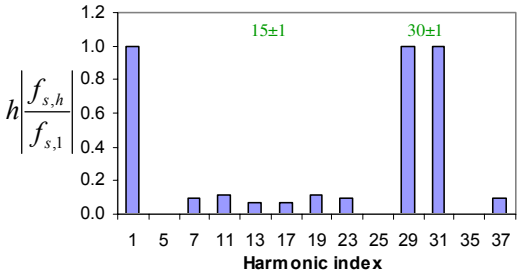

(b) Normalized stator mmf multiplied by harmonic index

Figure 4. Stator winding layout and the normalized stator mmf spectrum multiplied by the harmonic index h for n_s=15 with 2 poles.

Next, the less common case using odd-numbered values of n_s is considered. Figures 3a and 4a show the winding layouts for n_s=9 (spp=1.5) and n_s=15 (spp=2.5), respectively. Figure 3b and 4b show the normalized spectra of the spatial stator mmf distributions multiplied by the corresponding harmonic index h for comparison with Fig. 2b. Only the harmonic components with orders of ($6m$±1) that are capable of producing ripple torque are plotted. Slot harmonics are amplified by h to have the same amplitude as the fundamental regardless of whether n_s is even or odd. However, if n_s is odd-numbered, half of the stator slot harmonics are even-numbered, as indicated in Fig. 3b and 4b. Consequently, half of the stator slot harmonics cannot interact to produce ripple torque with the rotor mmf harmonics that are all odd-numbered.

For example, the set of slot harmonic orders for the case of n_s=9, includes 9±1, 18±1, 27±1, and 36±1. Among these orders, 9±1, 27±1, and all orders of kn_s±1 with odd values of k are even-numbered. As a result, half of the high-amplitude stator slot harmonic components are incapable of interacting with the rotor mmf harmonics to produce ripple torque. Adopting this technique to minimize the stator-rotor mmf harmonic interactions can significantly reduce the ripple torque. In the literature [4], the stator winding configuration with n_s=9 shown in Fig. 3a has been demonstrated to reduce the torque ripple amplitude for a surface permanent magnet (SPM) machine design.

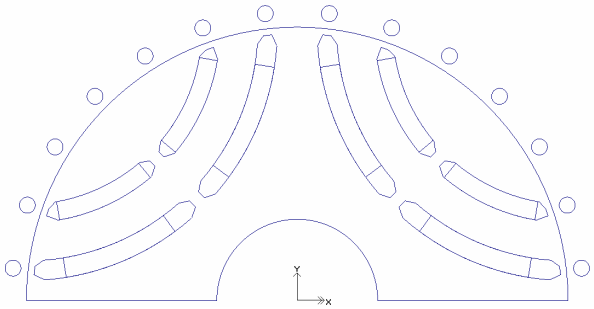

(a) Rotor cross section

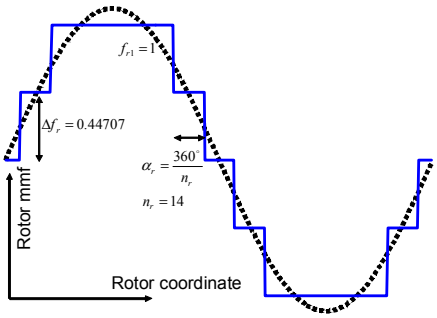

(b) Spatial distribution of rotor mmf

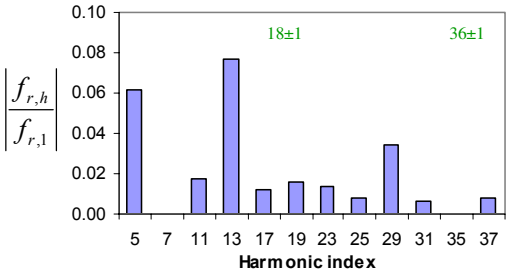

(c) Normalized spectrum of spatial rotor mmf distribution

Figure 5. The rotor design with two layers of flux barriers optimized with the stator winding configuration using n_s=9 (Design A)

IV. Proposed Analytical Rotor Design Approach

This section presents an analytical rotor design approach that minimizes the torque ripple index (TRI) in (17) when the stator winding configuration and the number of layers for the rotor flux barriers per pole are given. As the first example (Design A), an IPM machine configuration with n_s=9 slots-per-pole-pair in the stator (Fig. 3) and a rotor with two layers of flux barriers per pole (Fig. 5) is considered.

The proposed rotor design procedure consists of three steps: 1) Determine the optimal shape of the spatial rotor mmf distribution; 2) Determine the scaling (amplitude) of the rotor mmf under open-circuit and short-circuit conditions; and 3) Determine the geometrical shaping and sizing of the rotor flux barriers and permanent magnet source fluxes. The detailed description of each step follows in the subsections below.

Finally, the results of applying the proposed design procedure to a second machine configuration (Design B) with n_s=15 slots-per-pole-pair in the stator (Fig. 4) and a rotor with three layers of flux barriers per pole (Fig. 7) will be presented.

A. The Shape of Rotor MMF

The first step in the analytical rotor design is to find the best shape for the rotor mmf distribution that minimizes the amplitude of the torque ripple index *TRI* in (17). As illustrated in Figs. 5 and 7, IPM machines have step discontinuities in the rotor mmf spatial distributions due to the flux barriers. For rotors with two layers of flux barriers as shown in Fig. 5, there are two discrete steps per half pole for the rotor mmf values and two locations per half pole for the rotor bridges along the airgap surface (indicated as small circles in Fig. 5a).

Candidate rotor mmf shapes in this paper are constrained to have steps in their mmf values that are equal in amplitude and uniform pitch between neighboring rotor cavities as shown in Fig. 5b. Adoption of these constraints greatly simplifies the optimization problem and increases the geometrical feasibility of the rotor cavity configuration, but has little effect on the quality of the optimization results. As an example, the rotor illustrated in Fig 5a has its rotor cavities aligned with fourteen equally-divided locations (n_r =14) along the airgap surface. This variable n_r is defined as the rotor slot harmonic number.

Minimization of the value of *TRI* value under the two constraints listed above with n_s =9 leads to selection of n_r =14 as the preferred rotor slot harmonic number and a minimum *TRI* value of 0.064. The associated optimized rotor is shown in Fig. 5a and the corresponding mmf waveshape that minimizes the value of *TRI* is shown in Fig. 5b. Figures 5c plots the normalized harmonic spectrum of the optimized rotor mmf distribution. Only the harmonic components (h=6m±1) that interact with stator mmf harmonics of the same order to produce ripple torque are plotted in this figure. In order to achieve low torque ripple when combined with a stator winding using n_s =9, the rotor mmf harmonics must suppress the stator slot harmonics of orders 18±1, 36±1 as much as possible. Figure 5c illustrates how optimization of the rotor mmf harmonic distribution contributes to achieving this objective.

B. Fundamental Components of the Rotor MMF

Once the shape of the rotor mmf distribution is determined, the next step is to determine the fundamental component amplitudes for the stator mmf and the rotor mmf spatial waveforms. For this discussion, it is assumed that a preliminary machine design has been developed that meets all of the performance specifications identified in Table II without addressing any torque ripple requirements. The fundamental component amplitudes for this preliminary design are then used as the basis for developing new designs with reduced torque ripple.

The values of the fundamental amplitudes for the design specification used in this paper are tabulated in Table III. Items to note from this table include: 1) the fundamental component amplitude of the rotor mmf under open-circuit conditions determines the back-emf amplitude; 2) the fundamental component of the stator mmf under short-circuit conditions determines the characteristic current; and 3) the small difference between the rotor mmf and the stator mmf entries under short-circuit conditions is determined by the stator leakage inductance; and 4) the (short – open) condition corresponds to the case with *d*-axis stator current mmf acting alone with no magnet flux.

TABLE III. FUNDAMENTAL COMPONENT AMPLITUDES FOR THE STATOR MMF AND THE ROTOR MMF OF THE EXAMPLE IPM MACHINES

	$f_{s,1}$	$f_{r,1}$
Open circuit	0 [Apk*Turns]	218.9 [Apk*Turns]
Short circuit	534.6 [Apk*Turns]	629.5 [Apk*Turns]
Short – Open	534.6 [Apk*Turns]	410.6 [Apk*Turns]

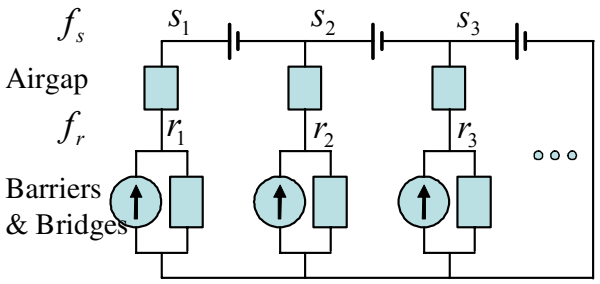

Figure 6. Magnetic circuit for a half pole of the IPM machine.

C. *Shape of Rotor Flux Barriers*

Following determination of the shape and the fundamental component amplitude of the rotor mmf, the next step is to solve the half-pole magnetic circuit in Fig. 6 to analytically determine the height, width, and the permanent magnet source flux of each flux barrier.

Key assumptions made for the magnetic circuit in Fig. 6 include the following: 1) No magnetic saturation is assumed in the bulk laminations; 2) A smooth airgap is assumed; 3) Each flux barrier and structural bridge is modeled by a parallel combination of a fixed flux source and a linear permeance made of air; and 4) the rotor axial length is unchanged from the value for the preliminary design.

The procedure for solving the magnetic circuit is described in a separate paper [9]. Interested readers are referred to this work for details on how to determine the height and width of the rotor magnet cavities. The resulting rotor geometry for Design A that realizes the optimal rotor mmf waveshape using the fundamental component amplitudes in Table III is shown in Fig. 5a.

D. *Second Example Machine (Design B)*

The proposed rotor design procedure is applied to a second example IPM machine that includes a stator winding configuration that uses n_s=15 slots-per-pole-pair (Fig. 4) and a rotor with three layers of flux barriers per pole. The results are presented in Fig. 7. For the rotors with three layers of flux barriers, there are three discrete steps in the rotor mmf waveform per half pole (Fig. 7b) and three locations per half pole for the rotor cavity ends along the airgap surface (marked with small circles in Fig. 7a).

Under the constraints of equal mmf step heights and uniform cavity pitches introduced earlier in this section, the optimized rotor mmf waveshape shown in Fig. 7b has the minimized *TRI* value of 0.02104 and a rotor slot harmonic number n_r=20. In order to achieve low torque ripple when paired with the stator winding of n_s =15, the rotor mmf harmonics should suppress the stator slot harmonics with orders of 30±1 to the greatest possible extent. The harmonic

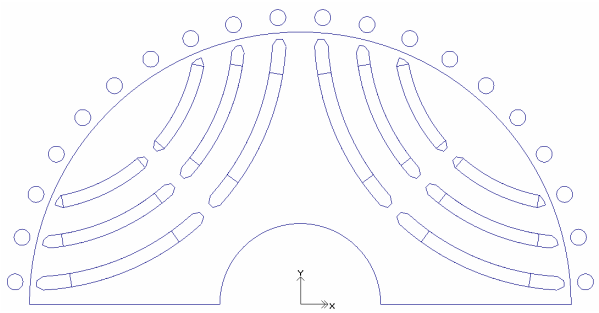

(a) Rotor cross section

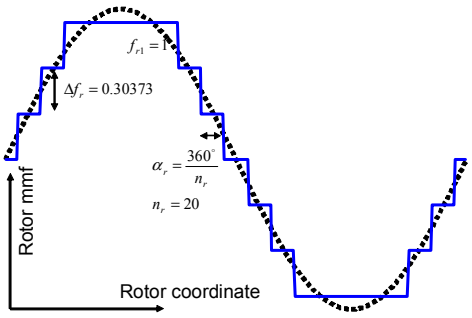

(b) Spatial distribution of rotor mmf

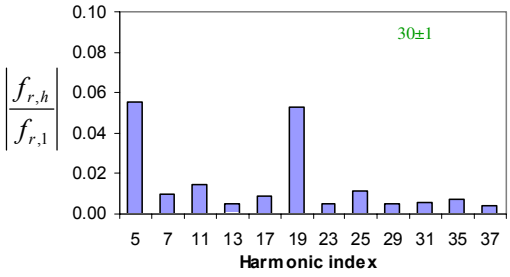

(c) Normalized spectrum of spatial rotor mmf distribution

Figure 7. Rotor design with three layers of flux barriers optimized with the stator winding configuration of n_s=15 (Design B)

spectrum of the rotor mmf waveform provided in Fig. 7c illustrates the effectiveness of the optimized rotor design in accomplishing this objective.

E. *Relationship to Prior Literature*

Before proceeding, a few comments are offered to provide some additional perspective about the IPM machine designs developed in this section with respect to other design results found in the technical literature. As noted earlier, the stator winding with n_s=9 shown in Fig. 3a has been used previously to reduce torque ripple for a surface permanent magnet (SPM) machine design [4]. The stator winding with n_s=15 shown in Fig. 4a represents an extension of the concept of applying stators with odd values of n_s to IPM machines.

A design rule has been proposed in [2] indicating that the preferred combination of stator and rotor slot harmonics for minimizing the ripple torque is n_s=n_r±4. However, only stators with even-numbered values of n_s were considered in [2]. It is interesting to note that, in contrast, the proposed design rule that emerges from the two example machines presented in this section is n_s=n_r–5 using odd-numbered values of n_s. The combination of n_s=n_r+5 is less attractive as an alternative

because of its poorer stator iron loss characteristics according to results presented in [9].

Moreover, the rotor design approach proposed in this paper calls for fewer layers of flux barriers per pole than [2] to realize the same rotor slot harmonic number n_r. For example, a rotor with n_r=14 is implemented with two layers of rotor cavities in this paper, whereas it is achieved with three layers in [2].

V. Finite Element Verification

Finite element (FE) analysis has been used to investigate the performance characteristics of the proposed design technique for minimizing torque ripple. More specifically, the Maxwell stress tensor method provided by commercial FE software has been used to calculate the instantaneous torque waveforms.

Figure 8 presents cross sections of the two example IPM machines that have been analyzed using the design results of the preceding section. Recalling, the first design (Design A) uses a stator winding configuration with n_s=9 and a rotor with n_r=14 and two layers of flux barriers per pole. The second design (Design B) uses a stator winding with a higher number of slots-per-pole-pair (n_s=15) and a rotor with n_r=20 and three layers of flux barriers per pole. Both designs meet the same performance specifications listed in Table II.

Figure 9 plots the calculated ratio of the peak-to-peak torque ripple to the average torque as a function of the current control angle measured from the *q*-axis with the rated current amplitude of 10 A_{pk}. Readers are again reminded that each result is presented as the ratio (in percent) of the peak-to-peak torque variation to the average torque *at the particular current angle operating point under investigation*. The results in Fig. 9 indicate that the torque ripple increases as the current control angle increases into the deep flux-weakening regime. This trend is consistent with (16) and published results in the literature [7].

The calculated torque ripple of Design A with two layers of rotor cavities falls into the range from 5.0% to 23.7%, while the calculate torque ripple of Design B with three cavity layers is in the range from 2.3% to 8.4%. Design A has its lowest torque ripple at a current angle of 10 degrees, while Design B has its lowest torque ripple at a current angle of 40 degrees. For both designs, maximum torque per ampere is achieved at a current angle of 40 degrees. For Design A, the predicted torque ripple at the maximum-torque-per-amp operating point is increased to 6.9% from its lowest value of 5.0%. In contrast, the maximum-torque-per-amp operating point delivers the lowest torque ripple of any current angle for Design B.

For IPM machines with two layers of flux barriers, the calculated torque ripple of 5.0% for the Design A machine is comparable to, but slightly greater than the lowest torque ripple levels found in the literature for two-layer machines [8]. The IPM machine in [8] combines two types of rotors into one hybrid rotor which is then step-skewed to suppress torque ripple. For IPM machines with three layers of flux barriers, the calculated torque ripple of 2.3% for the Design B machine is smaller than other values reported in the literature [2] for three-layer machines. The IPM machine in [2] uses a stator

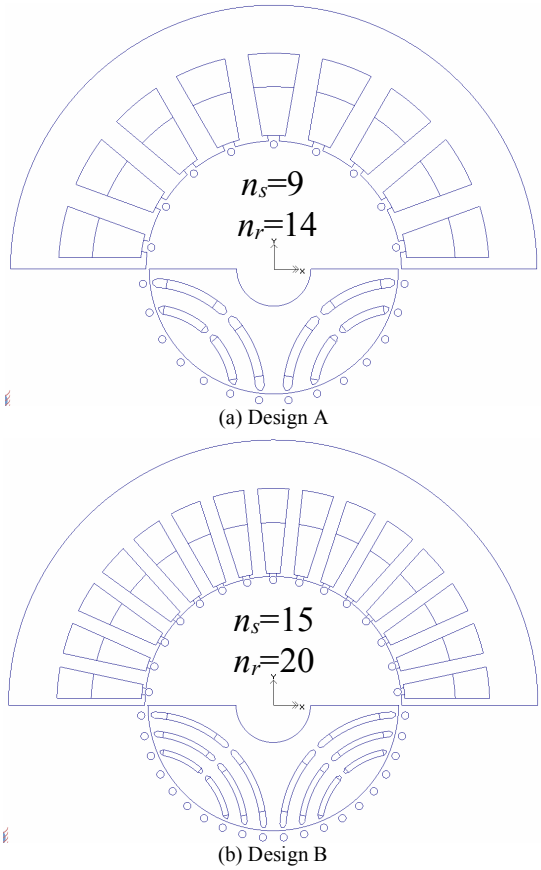

Figure 8. Cross sections of two example IPM designs: (a) Design A with n_s=9, n_r=14, and two layers of rotor flux barriers (b) Design B with n_s=15, n_r=20, and three layers of rotor flux barriers

configuration with n_s=18 combined with a three-layer rotor that uses n_r=14.

It should be noted that Designs A and B in Fig. 8 do not incorporate special techniques that have been reported to further reduce the torque ripple such as: 1) stator skewing; 2) novel variants of discrete rotor skewing [3],[8]; or 3) tailored shaping of the stator teeth or rotor poles [7].

Figure 10 displays the calculated instantaneous torque waveforms as a function of rotor position for several current angle values with the rated current amplitude of 10 A_{pk}. Examination of these waveforms indicates that a dominant harmonic order in the torque waveforms for Design A is 18 (period of 20 electrical degrees) while the torque waveforms for Design B contain a dominant harmonic order of 30 (period of 12 electrical degrees). In both machines, the dominant harmonic order of the torque ripple corresponds to $2n_s$. It can be noted that the base stator slot harmonic order of n_s did not contribute to the torque ripple because odd numbers were selected for n_s in both cases.

Another dominant harmonic order in the torque waveforms for both the Design A and B machines is 6, which corresponds to the phase-belt harmonic of the stator windings. The presence of these two dominant torque ripple harmonics at orders of $2n_s$ and 6 provide logical targets for future torque ripple reduction efforts.

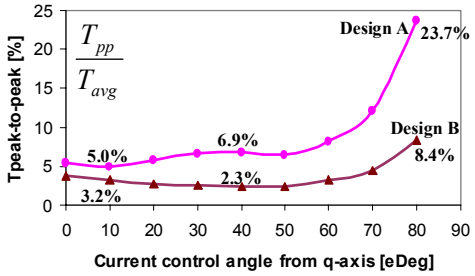

Figure 9. The percentage of the peak-to-peak torque ripple to the average torque as a function of the current control angle from q-axis with the rated current amplitude of 10 Apk

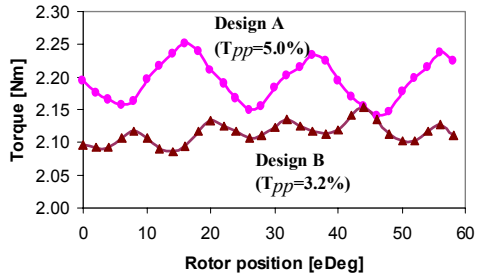

(a) 10 elec. degree current control angle from q-axis

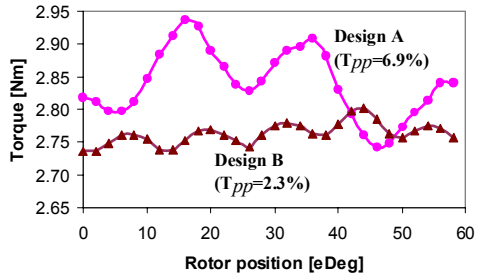

(b) 40 elec. degree current control angle from q-axis

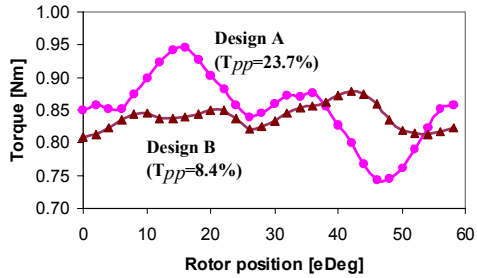

(c) 80 elec. degree current control angle from q-axis

Figure 10. The FE-calculated torque waveforms as a function of rotor position at different current control angles with respect to the q-axis with the rated current amplitude of 10 Apk

VI. Conclusions

This paper has presented a promising design approach for reducing the torque ripple in IPM machines by selecting the stator winding and rotor barrier configurations in carefully coordinated ways to minimize the overlap/interactions of their major mmf harmonic component orders. Key contributions of this paper include:

- An analytical expression has been developed for the torque ripple that clearly highlights the impact of the stator-rotor harmonic interactions and provides valuable insights for identifying alternative design improvements;
- These analytical results also demonstrate the advantage of selecting stator windings with odd numbers of slots-per-pole-pair to reduce stator-rotor mutual harmonic interactions;
- An analytical rotor design approach has been proposed that minimizes the torque ripple by guiding the designer to selection of the most promising configurations of the stator windings and rotor flux barriers;
- The proposed design concept has been demonstrated using finite element analysis carried out on two example IPM designs;

Taken together, these results provide promising evidence that low torque ripple can be achieved in IPM machines using relatively small numbers of stator slots and rotor flux barriers if the stator and rotor configurations are carefully designed in a coordinated fashion. Furthermore, the combined results show that the desired low torque ripple can be achieved for the full range of current control angles, including operation in the deep flux-weakening regime.

References

[1] D.W. Novotny and T.A. Lipo, *Vector Control and Dynamics of AC Drives*. Oxford, U.K.: Clarendon, 1998.

[2] A. Vagati, M. Pastorelli, G. Franceschini and S.C. Petrache, "Design of low-torque-ripple synchronous reluctance motors," *IEEE Trans. Ind. Appl.*, vol. 34, no. 4, pp. 758-765, July/Aug 1998.

[3] M. Sanada, K. Hiramoto, S. Morimoto and Y. Takeda, "Torque ripple improvement for synchronous reluctance motor using an asymmetric flux barrier arrangement," *IEEE Trans. Ind. Appl.*, vol. 40, no. 4, pp. 1076-82, Jul/Aug 2004.

[4] M.S. Islam, S. Mir, T. Sebastian and S. Underwood, "Design considerations of sinusoidally excited permanent-magnet machines for low-torque-ripple applications," *IEEE Trans. Ind. Appl.,* vol. 41, no. 4, pp. 955-962, July/Aug 2005.

[5] D.M. Ionel, M. Popescu, M.I. McGilp, T.J.E. Miller and S.J. Dellinger, "Assessment of torque components in brushless permanent-magnet machines through numerical analysis of the electromagnetic field," *IEEE Trans. Ind. Appl.*, vol. 41, no. 5, pp. 1149-1158, 2005.

[6] Sung-Il Kim, Ji-Young Lee, Young-Kyoun Kim, Jung-Pyo Hong, Y. Hur and Yeon-Hwan Jung, "Optimization for reduction of torque ripple in interior permanent magnet motor by using the Taguchi method," *IEEE Trans. Magn.*, vol. 41, no. 5, pp. 1796-9, May/June 2005.

[7] Sung-Il Kim, Ji-Hyung Bhan, Jung-Pyo Hong, and Ki-Chae Lim, "Optimization technique for improving torque performance of concentrated winding interior PM synchronous motor with wide speed range," in *Conf. Rec. of the 2006 IEEE IAS Annual Meeting*, Tampa, pp. 1933-1940, Oct. 2006.

[8] N. Bianchi, S. Bolognani, D. Bon, and M. Dai Pre, "Rotor flux-barrier design for torque ripple reduction in synchronous reluctance motors," in *Conf. Rec. of the 2006 IEEE IAS Annual Meeting*, Tampa, pp. 1193-1200, Oct. 2006.

[9] Seok-Hee Han, W.L. Soong, and T.M. Jahns, "An Analytical Design Approach for Reducing Stator Iron Losses in Interior PM Synchronous Machines during Flux-Weakening Operation," in *Conf. Rec. of the 2007 IEEE IAS Annual Meeting*, New Orleans, Sept. 2007.